

PAPER

CrossMark
click for updatesCite this: *Energy Environ. Sci.*,
2015, 8, 3637Unparalleled lithium and sodium superionic
conduction in solid electrolytes with large
monovalent cage-like anions†Wan Si Tang,^{*ab} Atsushi Unemoto,^c Wei Zhou,^a Vitalie Stavila,^d Motoaki Matsuo,^e
Hui Wu,^a Shin-ichi Orimo^{*ce} and Terrence J. Udovic^{*a}

Solid electrolytes with sufficiently high conductivities and stabilities are the elusive answer to the inherent shortcomings of organic liquid electrolytes prevalent in today's rechargeable batteries. We recently revealed a novel fast-ion-conducting sodium salt, $\text{Na}_2\text{B}_{12}\text{H}_{12}$, which contains large, icosahedral, divalent $\text{B}_{12}\text{H}_{12}^{2-}$ anions that enable impressive superionic conductivity, albeit only above its 529 K phase transition. Its lithium congener, $\text{Li}_2\text{B}_{12}\text{H}_{12}$, possesses an even more technologically prohibitive transition temperature above 600 K. Here we show that the chemically related $\text{LiCB}_{11}\text{H}_{12}$ and $\text{NaCB}_{11}\text{H}_{12}$ salts, which contain icosahedral, monovalent $\text{CB}_{11}\text{H}_{12}^-$ anions, both exhibit much lower transition temperatures near 400 K and 380 K, respectively, and truly stellar ionic conductivities ($>0.1 \text{ S cm}^{-1}$) unmatched by any other known polycrystalline materials at these temperatures. With proper modifications, we are confident that room-temperature-stabilized superionic salts incorporating such large polyhedral anion building blocks are attainable, thus enhancing their future prospects as practical electrolyte materials in next-generation, all-solid-state batteries.

Received 4th August 2015,
Accepted 8th October 2015

DOI: 10.1039/c5ee02941d

www.rsc.org/ees

Broader context

With the expanding interest in electric vehicles, the management of renewable energy, and other greener technologies in today's world, the need for improved energy-storage devices that deliver more power with higher capacities is ever increasing. Moreover, there is a growing desire to improve on the versatility, safety, and cycle-life afforded by the current device technologies, which typically incorporate organic-based liquid electrolytes. Hence there has been a general push to eliminate these liquid electrolytes in favor of all-solid-state devices using safe, stable, solid-state electrolytes. Until recently, the latter materials under consideration have been more ceramic or polymer-based. Complex-hydride materials, and more recently, large-polyhedral-anion-based materials such as $\text{LiCB}_{11}\text{H}_{12}$ and $\text{NaCB}_{11}\text{H}_{12}$ reported here are emerging as intriguing alternatives to these more traditional candidates. We believe that these newer types of solid-state electrolytes show great promise and deserve increased scrutiny as viable components of next-generation energy-storage devices.

Introduction

Based on their ability to form entropy-driven, cation- and anion-disordered structures, some complex hydride salts such as LiBH_4 and $\text{Na}_2\text{BH}_4\text{NH}_2$ have been found to exhibit impressive ionic conductivity,^{1,2} meriting their consideration as technologically

useful solid-state electrolytes^{3,4} and jumpstarting further efforts to find even more promising ionic conductors within this broad class of materials.⁵ More recently, the disordered phases of polyhedral boron-hydrogen compounds of Na containing the relatively stable dodecahydro-*closo*-dodecaborate ($\text{B}_{12}\text{H}_{12}^{2-}$) and decahydro-*closo*-decaborate ($\text{B}_{10}\text{H}_{10}^{2-}$) anions have proved to be quite remarkable superionic conductors,⁶⁻⁹ likely aided in part by the capacious interstitial corridors for cation transport afforded by the sublattice of unusually large quasispherical anions. Indeed, above their respective transition temperatures of $\approx 529 \text{ K}$ and 373 K , $\text{Na}_2\text{B}_{12}\text{H}_{12}$ exhibits a conductivity of 0.1 S cm^{-1} near 540 K ,⁸ whereas $\text{Na}_2\text{B}_{10}\text{H}_{10}$ exhibits a conductivity of 0.01 S cm^{-1} near 383 K .⁹ Both $\text{Li}_2\text{B}_{12}\text{H}_{12}$ and $\text{Li}_2\text{B}_{10}\text{H}_{10}$ have also been shown to undergo similar order-disorder transitions but only at temperatures well above 600 K , and although not yet confirmed, likely also become superionic.^{6,7,10,11}

^a NIST Center for Neutron Research, National Institute of Standards and Technology, Gaithersburg, MD 20899-6102, USA. E-mail: wansi.tang@nist.gov, udovic@nist.gov

^b Department of Materials Science and Engineering, University of Maryland, College Park, MD 20742-2115, USA

^c WPI-Advanced Institute for Materials Research (WPI-AIMR), Tohoku University, Sendai 980-8577, Japan. E-mail: orimo@imr.tohoku.ac.jp

^d Energy Nanomaterials, Sandia National Laboratories, Livermore, CA 94551, USA

^e Institute for Materials Research, Tohoku University, Sendai 980-8577, Japan

† Electronic supplementary information (ESI) available. See DOI: 10.1039/c5ee02941d

In spite of such compounds possessing the requisite conductivities for incorporation as electrolytes in next-generation, all-solid-state rechargeable batteries, it is highly desirable from a technology perspective to be able to stabilize the disordered superionic phase closer to or below room temperature, *e.g.*, *via* tailored chemical modifications that lead to either lower thermodynamically dictated ($T_{\text{trans}} \approx \Delta H_{\text{trans}}/\Delta S_{\text{trans}}$) phase-transition temperatures or a kinetics-inhibited low-temperature trapping of the high-temperature disorder. For instance, $\text{Na}_2\text{B}_{10}\text{H}_{10}$ can be considered as an anion-modified form of $\text{Na}_2\text{B}_{12}\text{H}_{12}$, yielding a smaller transition enthalpy change ΔH_{trans} and thus a lower T_{trans} , assuming a less-compound-dependent (order–disorder) entropy change ΔS_{trans} . Partially substituting Li for Na or halogenating the $\text{B}_{12}\text{H}_{12}^{2-}$ anion has also been shown to change the transition temperature, but in the opposite direction.¹² $\text{Na}_2\text{BH}_4\text{NH}_2$ is one example of a room-temperature fast-ion conductor enabled by a “freezing in” of its high-temperature disordered structure down to low temperatures.^{2,13} Another related example of trapping is the room-temperature stabilization of the high-temperature superionic disordered Na_3PS_4 phase by crystallization from glassy Na_3PS_4 .^{14,15}

One obvious chemical modification of potential interest involves the alteration of the $\text{B}_{12}\text{H}_{12}^{2-}$ anion itself. For example, replacing one {B–H} vertex with an isoelectronic {C–H} group yields the structurally similar icosahedral monocarba-*closo*-dodecaborate anion ($\text{CB}_{11}\text{H}_{12}^-$; see Fig. 1). The resulting reduced anion valency for $\text{CB}_{11}\text{H}_{12}^-$ compared to $\text{B}_{12}\text{H}_{12}^{2-}$ leads to a halving of the number of monovalent cations required for charge neutrality of the corresponding salt compounds, $\text{LiCB}_{11}\text{H}_{12}$ and $\text{NaCB}_{11}\text{H}_{12}$. A thorough review of the chemistry of the $\text{CB}_{11}\text{H}_{12}^-$ anion¹⁶ suggests that it is a relatively weakly binding and chemically inert anion,¹⁷ and indeed its potential as a viable liquid electrolyte component for Mg batteries has already been explored.¹⁸ Yet information on the properties of its anhydrous salt compounds is generally lacking. One study for $\text{CsCB}_{11}\text{H}_{12}$ reported an endothermic transition peak (upon heating) centered at around 564 K by differential scanning calorimetry (DSC) and confirmed a phase change by X-ray powder diffraction (XRPD) to what was suggested to be a high-temperature orthorhombic

structure.¹⁹ There was no clear evidence as to the nature of this supposedly disordered phase. Yet, based on an analogous structural study of $\text{Cs}_2\text{B}_{12}\text{H}_{12}$ (which exhibits a similar cation/anion size ratio),²⁰ such a phase does not necessarily possess any cation vacancies, which are paramount for fast-ion conduction. In contrast, our previous experience indicates that the formation of cation-vacancy-rich disordered structures with such large anions seems to be more common when the smaller Li^+ and Na^+ cations are involved.^{6,9,10} This proclivity likely has something to do with the smaller cations favoring lower cation coordination.^{11,12,21–23} In particular, the typical interstitial tetrahedral sites formed by the anions are too large for the diminutive Li^+ and Na^+ cations, forcing them to move laterally from the centers toward one of the four trigonal hollows to maximize their stability. Disorder transitions from these lower-coordination ordered structures tend to be of first-order and involve a dramatic increase in anion orientational mobility, which may further ameliorate the cation translational mobility within the anion sublattice.^{8,9,24} Hence, the potential effects of the different anion valency and 1:1 cation/anion ratio on T_{trans} and ionic conductivity, and the natures of the corresponding ordered and disordered $\text{LiCB}_{11}\text{H}_{12}$ and $\text{NaCB}_{11}\text{H}_{12}$ structures are intriguing and worthy of exploration.

In this paper, we report our results concerning the structural, dynamical, and conductive properties of $\text{LiCB}_{11}\text{H}_{12}$ and $\text{NaCB}_{11}\text{H}_{12}$. We have found respective transition temperatures of around 400 K and 380 K, which are substantially lower than those for the analogous $\text{Li}_2\text{B}_{12}\text{H}_{12}$ and $\text{Na}_2\text{B}_{12}\text{H}_{12}$ compounds. At room temperature, $\text{LiCB}_{11}\text{H}_{12}$ and $\text{NaCB}_{11}\text{H}_{12}$ exhibit ordered orthorhombic structures. Above these transition temperatures, the cation-vacancy-rich, disordered cubic phases for both compounds with their unusually high anion orientational mobility exhibit, to the best of our knowledge, unparalleled superionic Li^+ and Na^+ conductivities compared to the values reported for all other known solid polycrystalline materials at similar temperatures, polyhedral-anion-based or otherwise.

Experimental

For neutron scattering measurements, aqueous lithium and sodium monocarba-*closo*-dodecaborates $\text{LiCB}_{11}\text{H}_{12}$ and $\text{NaCB}_{11}\text{H}_{12}$ were each formed by first preparing $(\text{H}_3\text{O})\text{CB}_{11}\text{H}_{12}$ from trimethylammonium monocarba-*closo* dodecaborate $[(\text{CH}_3)_3\text{NH}]\text{CB}_{11}\text{H}_{12}$ (Katchem²⁵) by a procedure described in detail elsewhere,⁹ then neutralizing the $(\text{H}_3\text{O})\text{CB}_{11}\text{H}_{12}$ with either 0.1 M $^7\text{LiOH}$ (Cambridge Isotope Laboratories, 99.9+% ^7Li) or NaOH until a pH of 7 was reached. Finally, anhydrous $\text{LiCB}_{11}\text{H}_{12}$ and $\text{NaCB}_{11}\text{H}_{12}$ were obtained from these respective aqueous solutions, first using a rotary evaporator at room temperature to form a hydrated solid, followed by dehydration under vacuum at 433 K and 330 K, respectively, for 16 h. Boron-11 enrichment, although also desirable for neutron scattering measurements, was not considered in this study because of the added complication of needing ^{11}B -enriched starting materials to synthesize the $\text{CB}_{11}\text{H}_{12}^-$ anions. (*N.B.*, both ^6Li and ^{10}B present in natural Li and B are strong neutron absorbers).

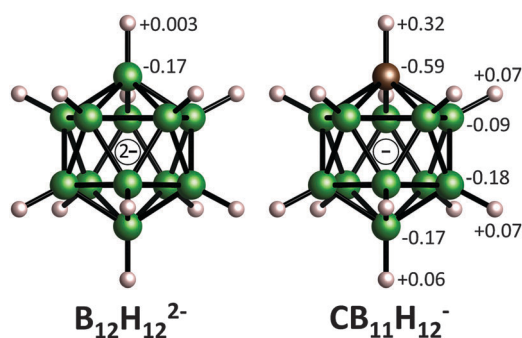


Fig. 1 Relative geometries of the $\text{B}_{12}\text{H}_{12}^{2-}$ and $\text{CB}_{11}\text{H}_{12}^-$ anions with boron, carbon, and hydrogen atoms denoted by green, brown, and white spheres, respectively. Numbers indicate the relative Mulliken charges associated with the structurally distinct atoms of the isolated anions as determined by first-principles calculations described in the text.

For all other non-neutron-related measurements, we used separate batches of $\text{LiCB}_{11}\text{H}_{12}$ (with no ^7Li enrichment) and $\text{NaCB}_{11}\text{H}_{12}$ obtained directly from Katchem.

Both anhydrous compounds were structurally characterized in quartz capillaries by XRPD using a Rigaku Ultima III X-ray diffractometer with a $\text{Cu-K}\alpha$ source ($\lambda = 1.5418 \text{ \AA}$). Elevated sample temperatures were enabled by a custom-designed, calibrated radiative/convective heat source. Differential scanning calorimetry measurements were made with a Netzsch (STA 449 F1 Jupiter) TGA-DSC under He flow with Al sample pans. Neutron scattering measurements were performed at the National Institute of Standards and Technology Center for Neutron Research. Neutron vibrational spectroscopy (NVS) measurements were performed at 4 K using thin flat-plate sample geometries and scattering in reflection on the Filter-Analyzer Neutron Spectrometer (FANS).²⁶ The $\text{Cu}(220)$ monochromator was used with pre- and post-collimations of $20'$ of arc, yielding a full-width-at-half-maximum (FWHM) energy resolution of about 3% of the neutron energy transfer. Quasielastic neutron scattering (QENS) measurements were performed using the same sample geometries on the Disc Chopper Spectrometer (DCS),²⁷ utilizing incident neutrons at 4.1 \AA (4.87 meV) with respective resolutions of $87.3 \mu\text{eV}$ and $184.4 \mu\text{eV}$ FWHM for $\text{NaCB}_{11}\text{H}_{12}$ and $\text{LiCB}_{11}\text{H}_{12}$. Spectra were collected in reflection over a useful momentum transfer (Q) range of around 1.0 \AA^{-1} to 2.88 \AA^{-1} . The instrument resolution function was determined from QENS spectra at 200 K. The neutron scattering data were analyzed using the DAVE software package.²⁸ XRPD structural refinements were performed using either GSAS²⁹ or Fullprof software.³⁰

Ionic conductivities were determined in heating and cooling runs repeatedly in the temperature range from room temperature to 433 K for $\text{LiCB}_{11}\text{H}_{12}$ and to 393 K for $\text{NaCB}_{11}\text{H}_{12}$ by the ac complex impedance method with a two-probe technique using a HIOKI 3532-80 chemical impedance meter over a frequency range of 4 Hz to 1 MHz with an input voltage perturbation of 150 mV. All measurements were performed under Ar. The powder sample was pressed into a pellet of 8 mm in diameter and approximately 2.7 mm in thickness without sintering. The pellet densities were about 1.05 g cm^{-3} and 1.13 g cm^{-3} , which are more than 94% of the densities calculated from the lattice parameters. Li and Au foils were used as electrodes for $\text{LiCB}_{11}\text{H}_{12}$ and $\text{NaCB}_{11}\text{H}_{12}$, respectively, and mechanically fixed onto both faces of the pellet.

$\text{LiCB}_{11}\text{H}_{12}$ was used in preliminary battery tests. TiS_2 (99.9%, Sigma-Aldrich) and $\text{LiCB}_{11}\text{H}_{12}$ powders were mixed in a 1:1 mass ratio by an agate mortar in an agate pestle, and then used as a composite positive electrode. 25 mg of $\text{LiCB}_{11}\text{H}_{12}$ and 6 mg of the composite positive electrode powders were separately placed in an 8 mm-diameter die and then uniaxially pressed at 190 MPa. Li foil was used as a negative electrode and placed opposite of the positive electrode. The assembled bulk-type, all-solid-state TiS_2/Li battery, namely $\text{TiS}_2/\text{LiCB}_{11}\text{H}_{12}|\text{LiCB}_{11}\text{H}_{12}|\text{Li}$, was placed in a stainless-steel electrochemical cell with an 8 mm-diameter Teflon[®] guide, as schematically illustrated elsewhere.³ All of the procedures for the battery assemblies were carried out in an Ar-filled glove box. The battery test was carried out at 403 K with a 0.2 C charge rate (C-rate), corresponding to

$285 \mu\text{A cm}^{-2}$, in the voltage range of 1.75 V to 2.6 V using a 580 battery test system (Scribner Associates).

To assist the structural refinements, first-principles calculations were performed within the plane-wave implementation of the generalized gradient approximation to Density Functional Theory (DFT) using a Vanderbilt-type ultrasoft potential with Perdew–Burke–Ernzerhof exchange correlation.³¹ A cutoff energy of 544 eV and a $2 \times 2 \times 1$ k -point mesh (generated using the Monkhorst–Pack scheme) were used and found to be enough for the total energy to converge within $0.01 \text{ meV atom}^{-1}$. For comparison with the NVS measurements, the phonon densities of states (PDOSs) were calculated from the DFT-optimized structures using the supercell method ($2 \times 2 \times 1$ cell size) with finite displacements.^{32,33} They were weighted to take into account the H, ^7Li , Na, C, and B total neutron scattering cross sections, appropriately averaged over Q -space, and convoluted with the instrumental resolution. The PDOS of the isolated $\text{CB}_{11}\text{H}_{12}^-$ anion was also calculated for comparison, using a $30 \times 30 \times 30$ supercell and full C_{5v} molecular symmetry. Mulliken atomic charges (shown in Fig. 1) were determined from these DFT calculations for the isolated $\text{CB}_{11}\text{H}_{12}^-$ anion as well as from those for the related $\text{B}_{12}\text{H}_{12}^{2-}$ anion using the same-size supercell and its full I_h molecular symmetry.

All structural depictions were made using the VESTA (Visualization for Electronic and Structural Analysis) software.³⁴ For all figures, standard uncertainties are commensurate with the observed scatter in the data, if not explicitly designated by vertical error bars.

Results and discussion

Fig. 2 shows DSC scans for $\text{LiCB}_{11}\text{H}_{12}$ and $\text{NaCB}_{11}\text{H}_{12}$, indicating a clear hysteretic phase change based on the respective endothermic (upon heating) and exothermic (upon cooling) enthalpic features. Here, they occur roughly near 395 K and 383 K for $\text{LiCB}_{11}\text{H}_{12}$

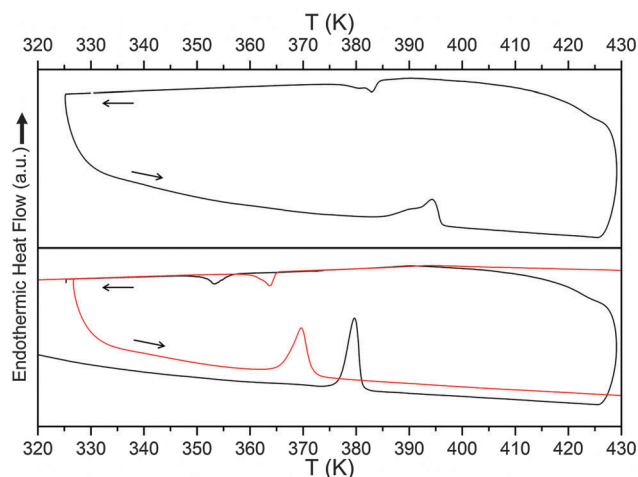


Fig. 2 Sequential heating (5 K min^{-1})/cooling ($\leq 2 \text{ K min}^{-1}$) DSC scans for (a) $\text{LiCB}_{11}\text{H}_{12}$ and (b) $\text{NaCB}_{11}\text{H}_{12}$ for two different cycles, the red curves measured after previously heating to 733 K. Arrows denote heating and cooling segments.

and near 380 K and 354 K for $\text{NaCB}_{11}\text{H}_{12}$, dramatically lower than their respective $\text{Li}_2\text{B}_{12}\text{H}_{12}$ and $\text{Na}_2\text{B}_{12}\text{H}_{12}$ analogs⁶ and suggestive of relatively lower enthalpic changes. As evidenced for $\text{NaCB}_{11}\text{H}_{12}$ during a later DSC cycle and for all the polyhedral borate salts, these temperatures can vary⁹ by more than 10 K depending on the cycling parameters and the maximum temperature employed, and seem to be intimately related to morphological changes that can occur with cycling, such as particle sintering or size reduction. We note that the inherent hystereses for these systems mean that the high-temperature phases can remain stable some degrees below the quoted T_{trans} values, which often refer to the values observed upon heating.

The room-temperature XRPD patterns and structural model fits for $\text{LiCB}_{11}\text{H}_{12}$ and $\text{NaCB}_{11}\text{H}_{12}$ are shown in Fig. 3. At room temperature, $\text{LiCB}_{11}\text{H}_{12}$ and $\text{NaCB}_{11}\text{H}_{12}$ were both indexed to orthorhombic structures. The approximate structural details for each compound were determined using direct space methods under the same most probable space group of Pca_21 (No. 29). DFT calculations were then individually performed to optimize the $\text{CB}_{11}\text{H}_{12}^-$ rigid-body geometries with respect to the relative C, B, and H positions. Final Rietveld structural refinements³⁵ of the lattice constants and cation and anion coordinates were

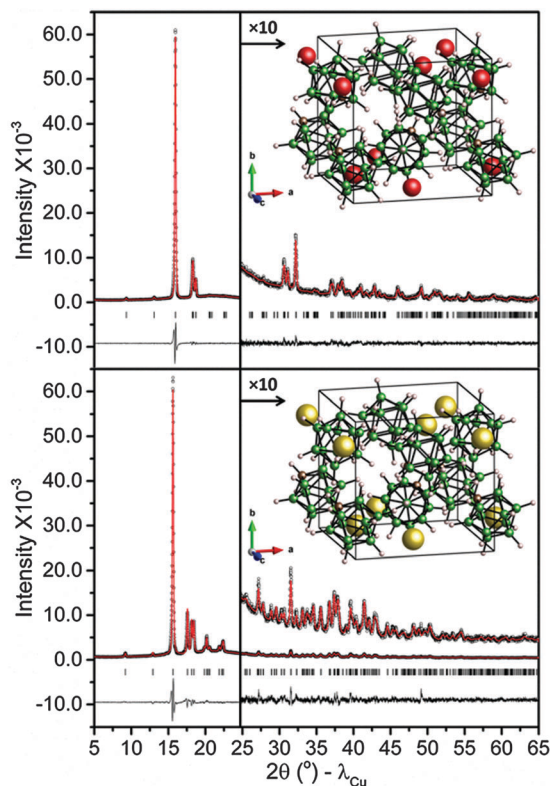


Fig. 3 Experimental (circles), fitted (line), and difference (line below observed and calculated patterns) XRPD profiles for orthorhombic $\text{LiCB}_{11}\text{H}_{12}$ (top) and $\text{NaCB}_{11}\text{H}_{12}$ (bottom) at room temperature ($\text{CuK}\alpha$ radiation). Vertical bars indicate the calculated positions of the Bragg peaks. $a = 9.6668(5)$ Å, $b = 9.4892(5)$ Å and $c = 9.7273(5)$ Å for $\text{LiCB}_{11}\text{H}_{12}$; $a = 9.7821(4)$ Å, $b = 9.6254(4)$ Å, and $c = 10.0928(4)$ Å for $\text{NaCB}_{11}\text{H}_{12}$. Insets depict the corresponding structures. Red, yellow, brown, green, and white spheres denote Li, Na, C, B, and H atoms, respectively.

carried out using the DFT-optimized $\text{CB}_{11}\text{H}_{12}^-$ rigid bodies. Full crystallographic details can be found in the CIF files in the ESI.†

The Fig. 3 insets depict the similar orthorhombic structures for $\text{LiCB}_{11}\text{H}_{12}$ and $\text{NaCB}_{11}\text{H}_{12}$. In both of these ordered structures, the C atoms are not orientationally disordered amongst the various icosahedral vertices. Rather, there is a preferred vertex position for the C atom within the structures. As can be seen in Fig. 1, although the C atom has a markedly larger negative Mulliken charge than the other B atoms of the $\text{CB}_{11}\text{H}_{12}^-$ anion, its covalently bonded H atom has about a fivefold larger positive Mulliken charge than those for the other B-bonded H atoms. This anomalously large positive charge has a major influence on the lowest-energy orientation established by the anion and the particular crystallographic position of its C atom. As such, it is most energetically favorable for these particular H atoms to maximize their distance from the surrounding cations,^{16,36} as is observed here both experimentally and by our DFT calculations.

The neutron vibrational spectra for $\text{LiCB}_{11}\text{H}_{12}$ and $\text{NaCB}_{11}\text{H}_{12}$ at 4 K are shown in Fig. 4 and are compared with the simulated PDOSs based on the DFT-optimized, XRPD-refined structures as well as that for the isolated $\text{CB}_{11}\text{H}_{12}^-$ anion. Due to the relatively large neutron scattering cross-section for H atoms compared to Li, Na, C, and B atoms, the spectrum is dominated by the various optical vibrational modes involving H-atom displacements. Hydrogen stretching modes are at higher energies and are outside the measured energy range. There is good agreement between the experimental and simulated spectra, providing

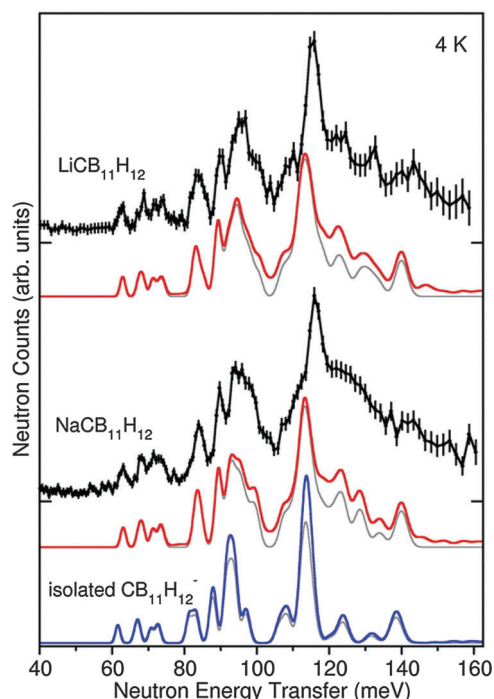


Fig. 4 Neutron vibrational spectra (black) of $\text{LiCB}_{11}\text{H}_{12}$ and $\text{NaCB}_{11}\text{H}_{12}$ at 4 K compared to the simulated one+two-phonon densities of states from first-principles phonon calculations of the optimized orthorhombic structures (red), and the isolated $\text{CB}_{11}\text{H}_{12}^-$ anion (blue). Simulated one-phonon densities of states are depicted in grey. (N.B., $1 \text{ meV} \approx 8.066 \text{ cm}^{-1}$.)

further credence to the refined structures. As suggested by the simulated PDOS of the isolated $\text{CB}_{11}\text{H}_{12}^-$ anion in Fig. 4 and borne out by PDOS results for other polyhedral hydroborate salts,³⁷ the neutron vibrational spectrum is typically found to be sensitive to the crystal structure arrangement.

Further information about the characters and energies of the different $\text{LiCB}_{11}\text{H}_{12}$ and $\text{NaCB}_{11}\text{H}_{12}$ phonon modes contributing to the simulated PDOSs can be found in the animation files in the ESI.†³⁸

Fig. 5 shows representative XRPD refinement results for the high-temperature disordered phase of $\text{LiCB}_{11}\text{H}_{12}$. (See Fig. S1 in the ESI,† for the $\text{NaCB}_{11}\text{H}_{12}$ refinement results.) Two different schematic views (lower inset and top) illustrate the primary disordered face-centered-cubic (fcc) structure found for both $\text{LiCB}_{11}\text{H}_{12}$ (at 430 K) and $\text{NaCB}_{11}\text{H}_{12}$ (at 356 K). The orientationally disordered anion arrangements are akin to the high-temperature disordered structures observed for $\text{Li}_2\text{B}_{12}\text{H}_{12}$,

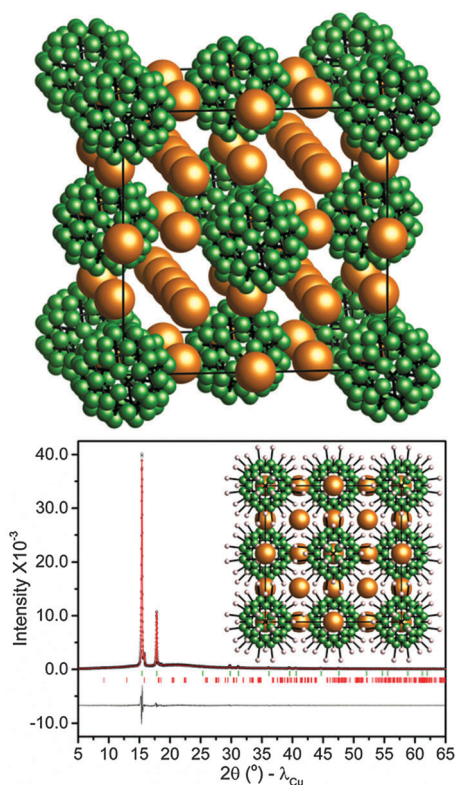


Fig. 5 (bottom) Experimental (circles), fitted (line), and difference (line below observed and calculated patterns) XRPD profiles for the high-temperature, disordered, face-centered-cubic (fcc) structure for $\text{LiCB}_{11}\text{H}_{12}$ at 430 K (CuK α radiation), with $a = 9.9355(6)$ Å. Vertical bars indicate the calculated positions of the Bragg peaks (with about 5% orthorhombic phase still present). $\text{NaCB}_{11}\text{H}_{12}$ at 356 K is isostructural with $a = 10.066(3)$ Å. Inset is a schematic view of the disordered structure along a principal axis. Orange, green, and white spheres denote Li/Na, C/B, and H atoms, respectively. (top) An alternate view without the H atoms, better indicating the cation channels. *N.B.*, the disordered cation positions reflect likely locations based on favorable interstitial volumes and previous neutron diffraction results for similarly disordered $\text{Na}_2\text{B}_{10}\text{H}_{10}$.^{9,21} Moreover, multiple distinct B/C and H positions are only meant to mimic the average, spherically isotropic, anion orientational disorder present in these materials.

$\text{Na}_2\text{B}_{10}\text{H}_{10}$, and one of the high-temperature polymorphs of $\text{Na}_2\text{B}_{12}\text{H}_{12}$,^{6,9} and provide a network of ample interstitial space with relatively more cation vacancies than $\text{Li}_2\text{B}_{12}\text{H}_{12}$ and $\text{Na}_2\text{B}_{12}\text{H}_{12}$ for facile cation transport. Although we observe only fcc structures at these temperatures, additional XRPD measurements indicate the gradual competing appearance of other similar-energy (and clearly similarly conductive) disordered polymorphs for $\text{NaCB}_{11}\text{H}_{12}$ at longer times and/or at higher temperatures (see Fig. S2 in the ESI†), which is not uncommon.⁶ It is possible that $\text{LiCB}_{11}\text{H}_{12}$ also possesses different polymorphs at higher temperatures above 430 K.

Preliminary QENS measurements for both $\text{LiCB}_{11}\text{H}_{12}$ and $\text{NaCB}_{11}\text{H}_{12}$ confirm the orders of magnitude leaps in anion orientational mobilities to between 10^{10} and 10^{11} reorientational jumps s^{-1} in the disordered phases, as reflected in Fig. 6 by the transformation from purely resolution-limited elastic component peaks at 200 K to ones with significant quasielastic broadening at 433 K and 375 K, respectively. For both materials, the observed fraction of scattering that is quasielastic above $Q = 1 \text{ \AA}^{-1}$ appears to be of the order of 0.8 or more, suggesting that we are observing anion small-angle-jump reorientations akin to that observed for $\text{Na}_2\text{B}_{12}\text{H}_{12}$,²⁴ which is thought to entail a distribution of individual anion motions ranging from one-axis to multi-axis

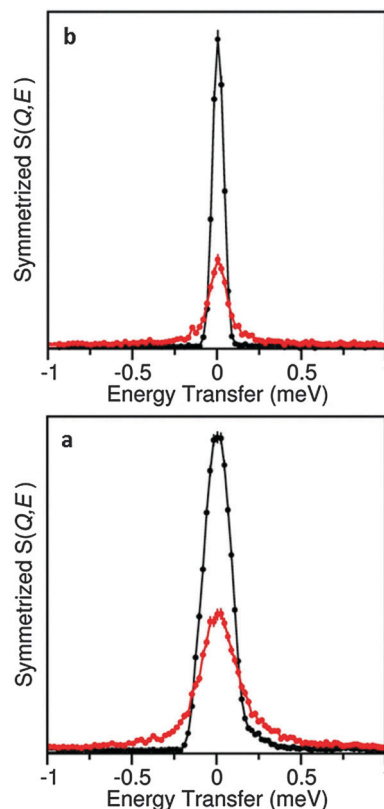


Fig. 6 QENS spectra at $Q = 1.35 \text{ \AA}^{-1}$ showing the anion-reorientation-induced broadening in red for (a) $\text{LiCB}_{11}\text{H}_{12}$ (at 433 K) and (b) $\text{NaCB}_{11}\text{H}_{12}$ (at 375 K) compared to the resolution-limited elastic-scattering peaks in black observed at 200 K, below the order-disorder phase transitions. (*N.B.*, lower instrumental resolution was used for $\text{LiCB}_{11}\text{H}_{12}$, as detailed in the Experimental section.)

reorientations. A comparison of a simple one-Lorentzian fit of the broad component for $\text{NaCB}_{11}\text{H}_{12}$ in Fig. 6b to that for $\text{Na}_2\text{B}_{10}\text{H}_{10}$ under identical conditions of temperature, Q , and instrumental resolution suggests that reorientational jump frequencies for the $\text{CB}_{11}\text{H}_{12}^-$ anions may be on the order of 60% higher than those for the $\text{B}_{10}\text{H}_{10}^{2-}$ anions.⁹ (*N.B.*, $\text{Na}_2\text{B}_{12}\text{H}_{12}$ is not normally in its disordered phase at 375 K and is therefore less straightforward to compare.) Of course, this comparison assumes similar reorientational mechanisms and ignores the reality that the mechanism-dependent broadening for these highly disordered anions is actually comprised of more than one Lorentzian component.²⁴ A more rigorous comparison and analysis confirming our observations awaits further QENS measurements using ¹¹B-enriched materials in combination with parallel NMR studies. If these higher relative $\text{CB}_{11}\text{H}_{12}^-$ orientational mobilities compared to the analogous $\text{B}_{10}\text{H}_{10}^{2-}$ (and $\text{B}_{12}\text{H}_{12}^{2-}$) anions are indeed the case, they are likely a consequence of relatively weaker cation–anion (coulombic)

interactions as well as, on average, one-half fewer near-neighbor cations for the $\text{CB}_{11}\text{H}_{12}^-$ anion.

Fig. 7 summarizes the conductivity-related results for both compounds. The ac impedance spectra of the symmetric cells for the $\text{LiCB}_{11}\text{H}_{12}$ and the $\text{NaCB}_{11}\text{H}_{12}$ electrolytes are characteristic of pure ionic conductors. (*N.B.*, characteristic of all these disordered polyhedral-anion-based compounds, the anions can be considered translationally immobile compared to the rapidly diffusing cations.^{7,9} Moreover, additional dc conductivity measurements indicate that electronic conduction is also relatively negligible, confirming near-unity cation transport numbers.) As shown in Fig. 7a, the Li-symmetric cell for $\text{LiCB}_{11}\text{H}_{12}$ had a parallel circuit of a resistor and a capacitor (semi-circle) at $T \leq 393$ K while only ohmic resistance appeared at $T \geq 403$ K. On the other hand, a spike appeared after the semi-circle or ohmic resistance when using a Au-symmetric cell with this electrolyte (Au-symmetric cell data not shown) as well as with the $\text{NaCB}_{11}\text{H}_{12}$ electrolyte (Fig. 7b) owing to interface resistance. Thus, the semi-circle and ohmic

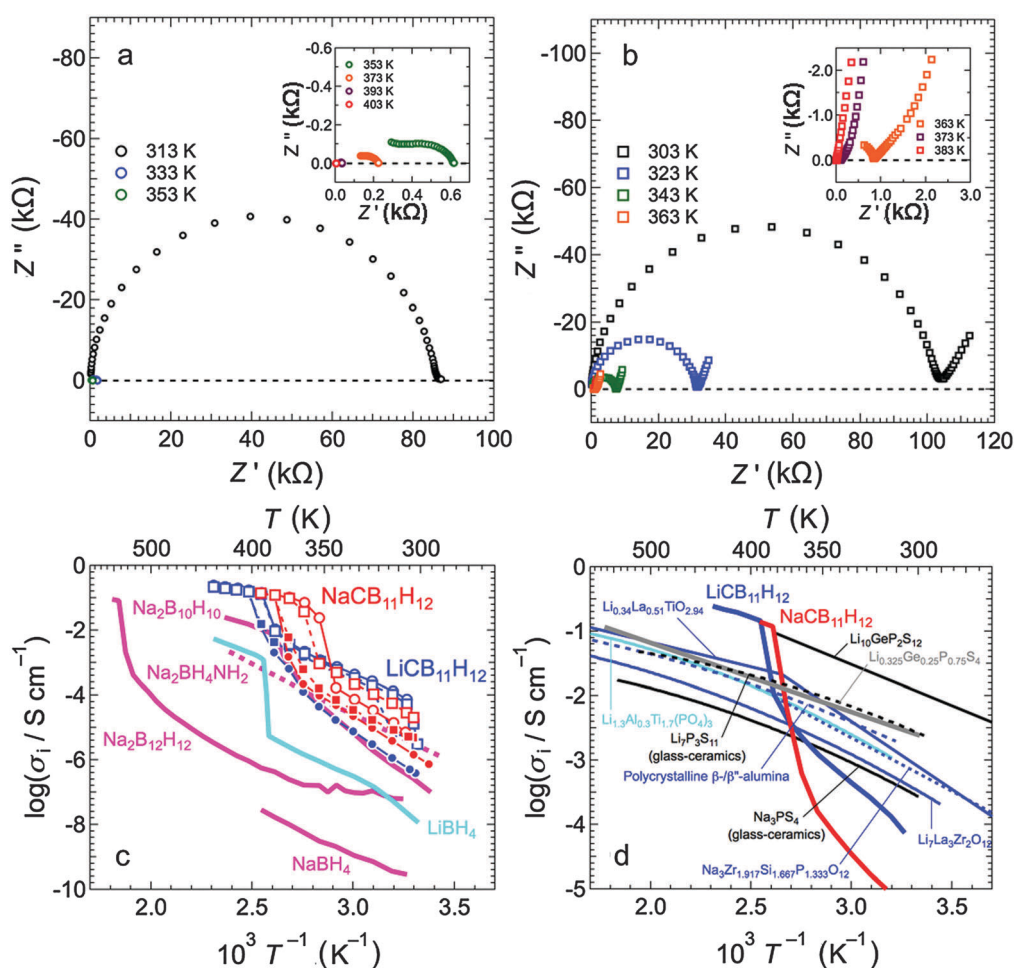


Fig. 7 Complex impedance plots of (a) Li-symmetric cell using the $\text{LiCB}_{11}\text{H}_{12}$ electrolyte and (b) Au-symmetric cell using the $\text{NaCB}_{11}\text{H}_{12}$ electrolyte measured at various temperatures during 2nd heating. (c) Ionic conductivities of species i ($i = \text{Li}^+$ and Na^+) of $\text{LiCB}_{11}\text{H}_{12}$ (blue) and $\text{NaCB}_{11}\text{H}_{12}$ (red) as a function of inverse temperature. Circles and squares denote the conductivities of the respective 1st and 2nd temperature cycles. Closed and open symbols denote respective heating and cooling processes. The ionic conductivities are compared to other related materials: $\text{Na}_2\text{B}_{12}\text{H}_{12}$,⁸ $\text{Na}_2\text{B}_{10}\text{H}_{10}$,⁹ $\text{Na}_2\text{BH}_4\text{NH}_2$,² NaBH_4 ,² and LiBH_4 .¹ (d) Comparison of ionic conductivities for $\text{LiCB}_{11}\text{H}_{12}$ and $\text{NaCB}_{11}\text{H}_{12}$ (during 2nd heating) with other known polycrystalline superionic conductors such as: $\text{Li}_{10}\text{GeP}_2\text{S}_{12}$,³⁹ $\text{Li}_7\text{P}_3\text{S}_{11}$ glass-ceramic,⁴¹ $\text{Li}_{0.325}\text{Ge}_{0.25}\text{P}_{0.75}\text{S}_4$,⁴² $\text{Li}_{0.34}\text{La}_{0.51}\text{TiO}_{2.94}$,⁴³ $\text{Li}_7\text{La}_3\text{Zr}_2\text{O}_{12}$,⁴⁴ $\text{Li}_{1.3}\text{Al}_{0.3}\text{Ti}_{1.7}(\text{PO}_4)_3$,⁴⁵ Na_3PS_4 glass-ceramic,¹⁴ polycrystalline β - β' -alumina mixture,⁴⁶ and $\text{Na}_3\text{Zr}_{1.917}\text{Si}_{1.667}\text{P}_{1.333}\text{O}_{12}$.⁴⁷

resistance appearing in the complex plane could be assigned to the total electrolyte resistances contributed by the bulk and grain boundaries. At elevated temperatures, conductivity jumps appeared for both materials accompanied by the order-disorder transition completed at 393 K to 403 K for $\text{LiCB}_{11}\text{H}_{12}$ and 373 K to 383 K for $\text{NaCB}_{11}\text{H}_{12}$. σ_{Li^+} for $\text{LiCB}_{11}\text{H}_{12}$ and σ_{Na^+} for $\text{NaCB}_{11}\text{H}_{12}$ are $\geq 0.15 \text{ S cm}^{-1}$ at $T \geq 403 \text{ K}$ and $\geq 0.12 \text{ S cm}^{-1}$ at $T \geq 383 \text{ K}$, respectively, with low activation energies of 0.22 eV. The high-temperature ionic conductivities are the greatest among polycrystalline electrolytes investigated thus far, complex hydrides (Fig. 7c) or otherwise (Fig. 7d). Indeed, Li^+ conductivity for $\text{LiCB}_{11}\text{H}_{12}$ appears to surpass even that of the best known material, $\text{Li}_{10}\text{GeP}_2\text{S}_{12}$ (which has a similar activation energy of 0.25 eV, Fig. 7d).³⁹ Na^+ conductivity for $\text{NaCB}_{11}\text{H}_{12}$ is even more impressive, being an order of magnitude higher than that of its closest competitor, $\text{Na}_2\text{B}_{10}\text{H}_{10}$,⁹ and almost 50× better (at 363 K) than the best Na_3PS_4 -based glass ceramic.^{14,40}

It should be noted that the intermediate conductivities observed between around 323 K and the higher-temperature transitions for both compounds in Fig. 7c upon temperature cycling are likely due to the premature formation or lingering of some superionic disordered material, as evidenced by parallel XRPD measurements during similar temperature-cycling algorithms. Such idiosyncrasies in the phase behaviors of the polyhedral borates are known to be sensitive to the particular morphological details of the materials.^{6,8,9}

The order-of-magnitude higher Na^+ conductivity for $\text{NaCB}_{11}\text{H}_{12}$ (and $\text{LiCB}_{11}\text{H}_{12}$) compared to $\text{Na}_2\text{B}_{10}\text{H}_{10}$, despite the similar high-temperature structures, is quite striking, leading one to reasonably speculate on the origins of such differences. Indeed, differences in anion charges, anion orientational mobilities, the number of cation vacancies, and lattice constants all might contribute to more favorable conductivities for the present compounds. In particular, the halved (monovalent) anion charge might lead to a decreased barrier for cation jumps through the anion sublattice due to decreased coulombic interactions. A relatively weaker Li^+ -anion interaction is indeed suggested for the $\text{CB}_{11}\text{H}_{12}^-$ anion from comparative mass spectrometry results and cluster calculations for both $\text{Li}_2\text{B}_{12}\text{H}_{12}$ and $\text{LiCB}_{11}\text{H}_{12}$ moieties.^{48,49} Also, the 1 : 1 cation : anion ratio means that there are relatively half as many cations in the $\text{LiCB}_{11}\text{H}_{12}$ and $\text{NaCB}_{11}\text{H}_{12}$ structures and therefore more available cation vacancies per unit cell. This would diminish the effects of possible cation-site blocking that might hinder cation transport. Moreover, the potentially more orientationally mobile $\text{CB}_{11}\text{H}_{12}^-$ anions might further assist cation transport by acting as better “lubricants” or cooperative (barrier-lowering) partners as cations attempt to move past them.^{8,24} Lastly, even though the $\text{CB}_{11}\text{H}_{12}^-$ and $\text{B}_{10}\text{H}_{10}^{2-}$ anions are of similar size, the fcc lattice constant for $\text{NaCB}_{11}\text{H}_{12}$ at 356 K is already over 2% larger than that for $\text{Na}_2\text{B}_{10}\text{H}_{10}$ at 410 K,²¹ possibly providing a little more space for cation transport. As a result of all these factors, the Li^+ and Na^+ cations more rapidly migrate through the vacancy-rich three-dimensional sublattices of the high-symmetry cubic crystal structures that prevail in these materials. Hence, Both $\text{LiCB}_{11}\text{H}_{12}$ and $\text{NaCB}_{11}\text{H}_{12}$ exhibit liquid-like high ionic conductivities, as in the classical silver superionic

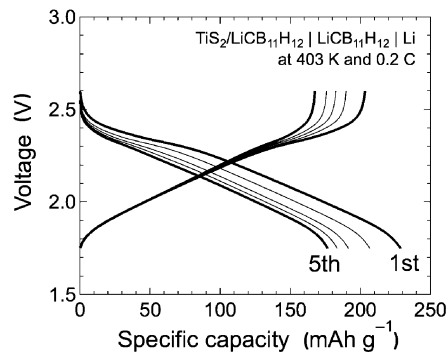


Fig. 8 Discharge-charge profiles over five cycles of the bulk-type all-solid-state 50 wt% $\text{TiS}_2/\text{LiCB}_{11}\text{H}_{12}|\text{LiCB}_{11}\text{H}_{12}|\text{Li}$ battery operated at 403 K and 0.2 C.

conductor, $\alpha\text{-AgI}$ ($\sigma_{\text{Ag}^+} \geq 1.3 \text{ S cm}^{-1}$ at $T \geq 420 \text{ K}$).^{50,51} A clearer understanding of the roles and importance of these various factors on the ultimate conductivity attainable in the superionic phases of this general class of compounds still awaits a thorough theoretical analysis of the different solid-state disordered systems accompanied by more experimental studies.

As a representative test of electrochemical stability, $\text{LiCB}_{11}\text{H}_{12}$ was incorporated into a positive electrode layer comprised of a hand-mixed $\text{TiS}_2/\text{LiCB}_{11}\text{H}_{12}$ powder in a 1 : 1 mass ratio. This positive electrode layer was part of a bulk-type, all-solid-state $\text{TiS}_2/\text{LiCB}_{11}\text{H}_{12}|\text{LiCB}_{11}\text{H}_{12}|\text{Li}$ battery with $\text{LiCB}_{11}\text{H}_{12}$ acting as the electrolyte separator. This cell was operated repeatedly at 403 K and 0.2 C. It had approximately 175 mAh g^{-1} discharge capacity during operation with approximately 95% coulombic efficiency (ratio of discharge to charge capacities) after the 3rd cycle. Fig. 8 illustrates discharge-charge profiles over five cycles, which suggest that the $\text{LiCB}_{11}\text{H}_{12}$ is reasonably stable with respect to TiS_2 and Li over this voltage range. We consider this first rudimentary attempt to incorporate $\text{LiCB}_{11}\text{H}_{12}$ into a working battery as promising. As with all other new solid electrolyte materials, clearly many more electrochemical studies are warranted and need to be done to determine the optimal battery chemistries, configurations, and cycling conditions that can take full advantage of these polyhedral-anion-based salts, which is beyond the scope of this paper. Nonetheless, these preliminary results suggest that, besides their impressive conductivities, this class of complex hydrides comprised of highly stable aromatic-like⁵² polyhedral anions, including $\text{B}_{12}\text{H}_{12}^{2-}$, $\text{B}_{10}\text{H}_{10}^{2-}$, and $\text{CB}_{11}\text{H}_{12}^-$, has the potential for good electrochemical compatibility with commercial cathode materials, which will be critical for any eventual use in next generation, all-solid-state batteries.

Conclusions

This work shows that $\text{LiCB}_{11}\text{H}_{12}$ and $\text{NaCB}_{11}\text{H}_{12}$ undergo order-disorder phase transitions near 400 K and 380 K, respectively, which are substantially lower than those for the analogous $\text{Li}_2\text{B}_{12}\text{H}_{12}$ and $\text{Na}_2\text{B}_{12}\text{H}_{12}$ compounds. Above these transition temperatures, the cation-vacancy-rich, disordered phases for both compounds with their unusually high anion orientational mobility exhibit

unparalleled superionic Li⁺ and Na⁺ conductivities compared to the values reported for all other known solid polycrystalline Li⁺ and Na⁺ conducting materials.

Concerning other ongoing tangential studies, we have found that the stability range of the disordered phases for the broad class of polyhedral borate materials including the present materials can potentially be extended to lower temperatures *via* ball-milling, the details of which will be the subject of a separate publication. These morphological modifications can lead to dramatically improved bulk conductivities down to room temperature and below. Hence, the room-temperature conductivities of ball-milled LiCB₁₁H₁₂ and NaCB₁₁H₁₂ compounds have the potential to benefit significantly from the presence of such stabilized phases, and experiments are currently underway to explore this further.

Based on our current and past findings and the potential for further improvements *via* an assortment of possible additional morphological, chemical, or substitutional modifications, we believe that there are a large variety of intriguing new compounds and hybrid materials involving such large polyhedral anions still to be explored, and we anticipate that an optimized electrolyte from this class of materials will be considered one of the more promising for use in future, all-solid-state, energy conversion and storage devices.

Author contributions

W.S.T. performed the XRPD and DSC measurements/analyses. V.S. performed the sample syntheses/analyses. W.Z. performed the DFT calculations. H.W. also performed XRPD analyses. A.U. performed the battery test/analysis. M.M. performed the conductivity measurements/analysis. S.O. organized the electrochemical tests. T.J.U. initiated the study, performed the neutron scattering measurements/analyses, and wrote the paper with contributions from all other authors.

Acknowledgements

This work was performed, in part, in collaboration between members of IEA HIA Task 32-Hydrogen-based Energy Storage. The authors gratefully acknowledge support from DOE EERE through Grant No. DE-EE0002978; the Integrated Materials Research Center for the Low-Carbon Society (LC-IMR), Tohoku University; the Advanced Low Carbon Technology Research and Development Program (ALCA) from the Japan Science and Technology Agency (JST); and JSPS KAKENHI under Grant Nos. 25220911 and 26820311. This work utilized facilities supported in part by the NSF under Agreement No. DMR-0944772. The authors thank J. B. Leão for his technical assistance with the elevated-temperature XRPD measurements.

References

1 M. Matsuo, Y. Nakamori, S. Orimo, H. Maekawa and H. Takamura, *Appl. Phys. Lett.*, 2007, **91**, 224103.

- 2 M. Matsuo, S. Kuromoto, T. Sato, H. Oguchi, H. Takamura and S. Orimo, *Appl. Phys. Lett.*, 2012, **100**, 203904.
- 3 A. Unemoto, S. Yasaku, G. Nogami, M. Tazawa, M. Taniguchi, M. Matsuo, T. Ikeshoji and S. Orimo, *Appl. Phys. Lett.*, 2014, **105**, 083901.
- 4 M. Matsuo and S. Orimo, *Adv. Energy Mater.*, 2011, **1**, 161–172.
- 5 A. Unemoto, M. Matsuo and S. Orimo, *Adv. Funct. Mater.*, 2014, **24**, 2267–2279.
- 6 N. Verdal, J.-H. Her, V. Stavila, A. V. Soloninin, O. A. Babanova, A. V. Skripov, T. J. Udovic and J. J. Rush, *J. Solid State Chem.*, 2014, **212**, 81–91.
- 7 A. V. Skripov, O. A. Babanova, A. V. Soloninin, V. Stavila, N. Verdal, T. J. Udovic and J. J. Rush, *J. Phys. Chem. C*, 2013, **117**, 25961–25968.
- 8 T. J. Udovic, M. Matsuo, A. Unemoto, N. Verdal, V. Stavila, A. V. Skripov, J. J. Rush, H. Takamura and S. Orimo, *Chem. Commun.*, 2014, **50**, 3750–3752.
- 9 T. J. Udovic, M. Matsuo, W. S. Tang, H. Wu, V. Stavila, A. V. Soloninin, R. V. Skoryunov, O. A. Babanova, A. V. Skripov, J. J. Rush, A. Unemoto, H. Takamura and S. Orimo, *Adv. Mater.*, 2014, **26**, 7622–7626.
- 10 M. Paskevicius, M. P. Pitt, D. H. Brown, D. A. Sheppard, S. Chumphongphan and C. E. Buckley, *Phys. Chem. Chem. Phys.*, 2013, **15**, 15825–15828.
- 11 H. Wu, W. S. Tang, V. Stavila, W. Zhou, J. J. Rush and T. J. Udovic, *J. Phys. Chem. C*, 2015, **119**, 6481–6487.
- 12 W. S. Tang, T. J. Udovic and V. Stavila, *J. Alloys Compd.*, 2015, **645**, S200–S204.
- 13 A. V. Soloninin, O. A. Babanova, E. Y. Medvedev, A. V. Skripov, M. Matsuo and S. Orimo, *J. Phys. Chem. C*, 2014, **118**, 14805–14812.
- 14 A. Hayashi, K. Noi, A. Sakuda and M. Tatsumisago, *Nat. Commun.*, 2012, **3**, 856.
- 15 N. Tanibata, K. Noi, A. Hayashi, N. Kitamura, Y. Idemoto and M. Tatsumisago, *ChemElectroChem*, 2014, **1**, 1130–1132.
- 16 C. Douvris and J. Michl, *Chem. Rev.*, 2013, **113**, PR179–PR233.
- 17 K. Shelly and C. A. Reed, *J. Am. Chem. Soc.*, 1986, **108**, 3118–3120.
- 18 O. Tutusaus, R. Mohtadi, T. S. Arthur, F. Mizuno, E. G. Nelson and Y. V. Sevryugina, *Angew. Chem., Int. Ed.*, 2015, **54**, 7900–7904.
- 19 A. M. Romerosa, *Thermochim. Acta*, 1993, **217**, 123–128.
- 20 N. Verdal, H. Wu, T. J. Udovic, V. Stavila, W. Zhou and J. J. Rush, *J. Solid State Chem.*, 2011, **184**, 3110–3116.
- 21 H. Wu, W. S. Tang, W. Zhou, V. Stavila, J. J. Rush and T. J. Udovic, *CrystEngComm*, 2015, **17**, 3533–3540.
- 22 J.-H. Her, M. Yousufuddin, W. Zhou, S. S. Jalisatgi, J. G. Kulleck, J. A. Zan, S.-J. Hwang, R. C. Bowman Jr. and T. J. Udovic, *Inorg. Chem.*, 2008, **47**, 9757–9759.
- 23 J.-H. Her, W. Zhou, V. Stavila, C. M. Brown and T. J. Udovic, *J. Phys. Chem. C*, 2009, **113**, 11187–11189.
- 24 N. Verdal, T. J. Udovic, V. Stavila, W. S. Tang, J. J. Rush and A. V. Skripov, *J. Phys. Chem. C*, 2014, **118**, 17483–17489.
- 25 The mention of all commercial suppliers in this paper is for clarity and does not imply the recommendation or endorsement of these suppliers by NIST.

- 26 T. J. Udovic, C. M. Brown, J. B. Leão, P. C. Brand, R. D. Jiggetts, R. Zeitoun, T. A. Pierce, I. Peral, J. R. D. Copley, Q. Huang, D. A. Neumann and R. J. Fields, *Nucl. Instrum. Methods Phys. Res., Sect. A*, 2008, **588**, 406–413.
- 27 J. R. D. Copley and J. C. Cook, *Chem. Phys.*, 2003, **292**, 477–485.
- 28 R. T. Azuah, L. R. Kneller, Y. Qiu, P. L. W. Tregenna-Piggott, C. M. Brown, J. R. D. Copley and R. M. Dimeo, *J. Res. Natl. Inst. Stand. Technol.*, 2009, **114**, 341–358.
- 29 A. C. Larson and R. B. Von Dreele, *General Structure Analysis System*, Report LAUR 86-748; (Los Alamos National Laboratory, NM, 1994).
- 30 J. Rodriguez-Carvajal, *Physica B*, 1993, **192**, 55–69.
- 31 P. Giannozzi, *et al.*, *J. Phys.: Condens. Matter*, 2009, **21**, 395502.
- 32 G. Kresse, J. Furthmuller and J. Hafner, *Europhys. Lett.*, 1995, **32**, 729–734.
- 33 T. Yildirim, *Chem. Phys.*, 2000, **261**, 205–216.
- 34 K. Momma and F. Izumi, *J. Appl. Crystallogr.*, 2011, **44**, 1272–1276.
- 35 H. M. Rietveld, *J. Appl. Crystallogr.*, 1969, **2**, 65–71.
- 36 I. Zharov, T. Weng, A. Orendt, D. Barich, J. Penner-Hahn, D. Grant, Z. Havlas and J. Michl, *J. Am. Chem. Soc.*, 2004, **126**, 12033–12046.
- 37 N. Verdál, W. Zhou, V. Stavila, J.-H. Her, M. Yousufuddin, T. Yildirim and T. J. Udovic, *J. Alloys Compd.*, 2011, **509S**, S694–S697.
- 38 Phonon animation files in the ESI† for the DFT-optimized 0 K orthorhombic LiCB₁₁H₁₂ and NaCB₁₁H₁₂ structures can be viewed using the V_Sim software at http://inac.cea.fr/L_Sim/V_Sim/.
- 39 N. Kamaya, K. Homma, Y. Yamakawa, M. Hirayama, R. Kanno, M. Yonemura, T. Kamiyama, Y. Kato, S. Hama, K. Kawamoto and A. Mitsui, *Nat. Mater.*, 2011, **10**, 682–686.
- 40 K. B. Hueso, M. Armand and T. Rojo, *Energy Environ. Sci.*, 2013, **6**, 734–749.
- 41 F. Mizuno, A. Hayashi, K. Tadanaga and M. Tatsumisago, *Adv. Mater.*, 2005, **17**, 918–921.
- 42 R. Kanno and M. Murayama, *J. Electrochem. Soc.*, 2001, **148**, A742–A746.
- 43 Y. Inaguma, C. Lique, M. Itoh and T. Nakamura, *Solid State Commun.*, 1993, **86**, 689–693.
- 44 R. Murugan, V. Thangadurai and W. Weppner, *Angew. Chem., Int. Ed.*, 2007, **46**, 7778–7781.
- 45 H. Aono, E. Sugimoto, Y. Sadaoka, N. Imanaka and G. Adachi, *J. Electrochem. Soc.*, 1989, **136**, 590–591.
- 46 A. Hooper, *J. Phys. D: Appl. Phys.*, 1977, **10**, 1487–1496.
- 47 O. Bohnke, S. Ronchetti and D. Mazza, *Solid State Ionics*, 1999, **122**, 127–136.
- 48 J. Z. Dávalos, J. González, A. Guerrero, D. Hnyk, J. Holub and J. M. Oliva, *J. Phys. Chem. C*, 2013, **117**, 1495–1501.
- 49 S. Giri, S. Behera and P. Jena, *Angew. Chem., Int. Ed.*, 2014, **53**, 13916–13919.
- 50 C. Tubandt and E. Lorenz, *Z. Phys. Chem.*, 1914, **24**, 513–543.
- 51 K. Funke, *Prog. Solid State Chem.*, 1976, **11**, 345–402.
- 52 W. H. Lipscomb, *Boron Hydrides*, W. A. Benjamin, Inc., New York, 1963.

Electronic Supplementary Information for:

Unparalleled Lithium and Sodium Superionic Conduction in Solid Electrolytes with Large Monovalent Cage-like Anions

Wan Si Tang,^{*,a,b} Atsushi Unemoto,^c Wei Zhou,^a Vitalie Stavila,^d Motoaki Matsuo,^e Hui Wu,^a Shin-ichi Orimo,^{*,c,e} and Terrence J. Udovic^{*,a}

^aNIST Center for Neutron Research, National Institute of Standards and Technology, Gaithersburg, MD 20899-6102, USA

^bDepartment of Materials Science and Engineering, University of Maryland, College Park, MD 20742-2115, USA

^cWPI-Advanced Institute for Materials Research (WPI-AIMR), Tohoku University, Sendai 980-8577, Japan

^dEnergy Nanomaterials, Sandia National Laboratories, Livermore, CA 94551, USA

^eInstitute for Materials Research, Tohoku University, Sendai 980-8577, Japan

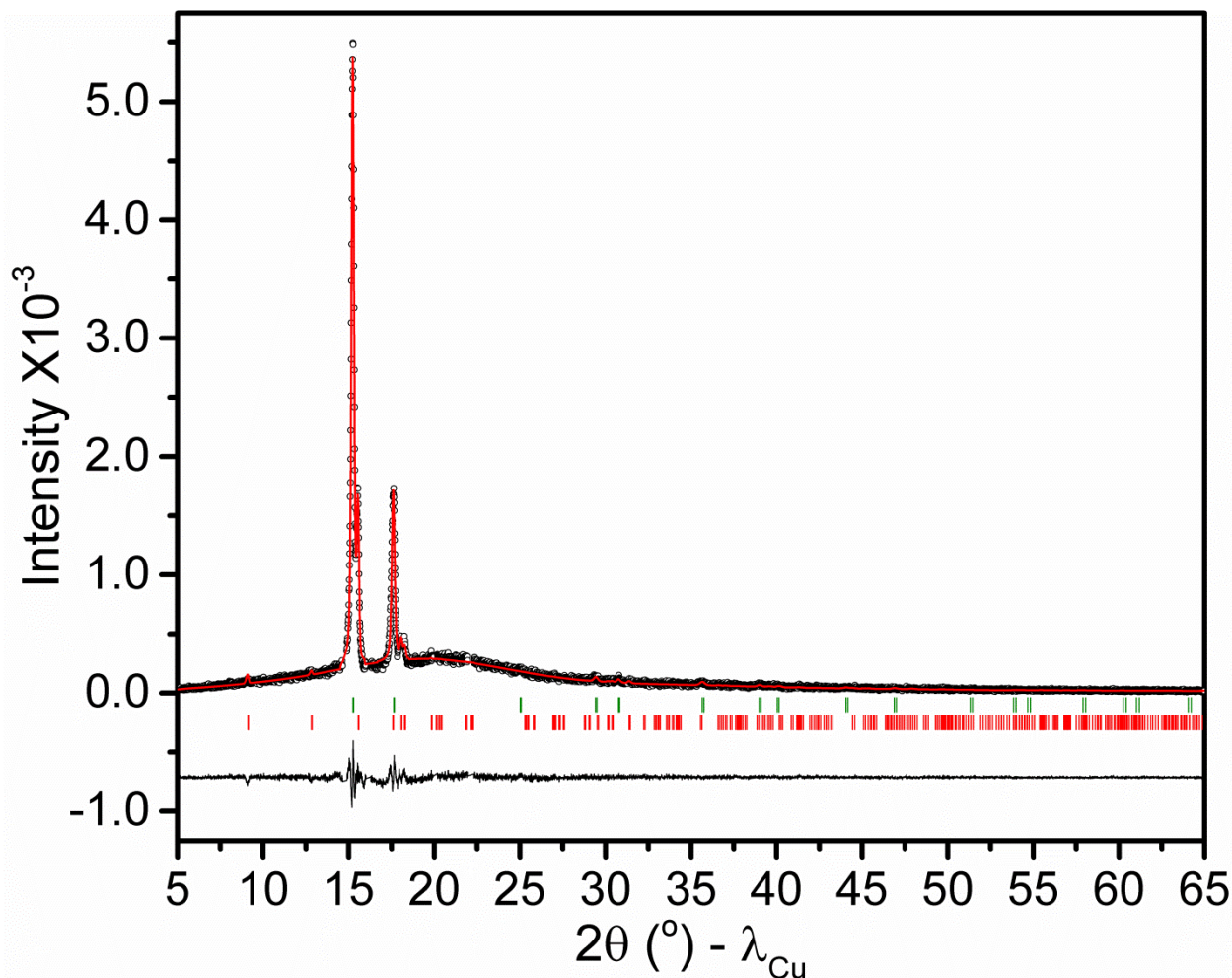


Fig. S1. Experimental (circles), fitted (line), and difference (line below observed and calculated patterns) XRPD profiles for $\text{NaCB}_{11}\text{H}_{12}$ at 356 K (CuK α radiation). Vertical bars indicate the calculated positions of Bragg peaks for the high-temperature fcc (77.8(1) wt. %) and the low-temperature orthorhombic phases (22.2(2) wt. %) of $\text{NaCB}_{11}\text{H}_{12}$, respectively (from the top). $R_{\text{wp}}=0.0782$, $R_p=0.0678$, $\chi^2=1.444$. The refined lattice parameter of the high-temperature fcc phase is 10.066(3) Å; and $a=9.818(3)$ Å, $b=9.712(4)$ Å, and $c=10.101(3)$ Å for the low-temperature orthorhombic phase. As for $\text{LiCB}_{11}\text{H}_{12}$ in Fig. 5, the refinement model for the fcc phase ignored the cations and H atoms and employed multiple B/C positions to mimic a spherical shell of B/C scatterers due to the isotropically orientationally disordered anions.

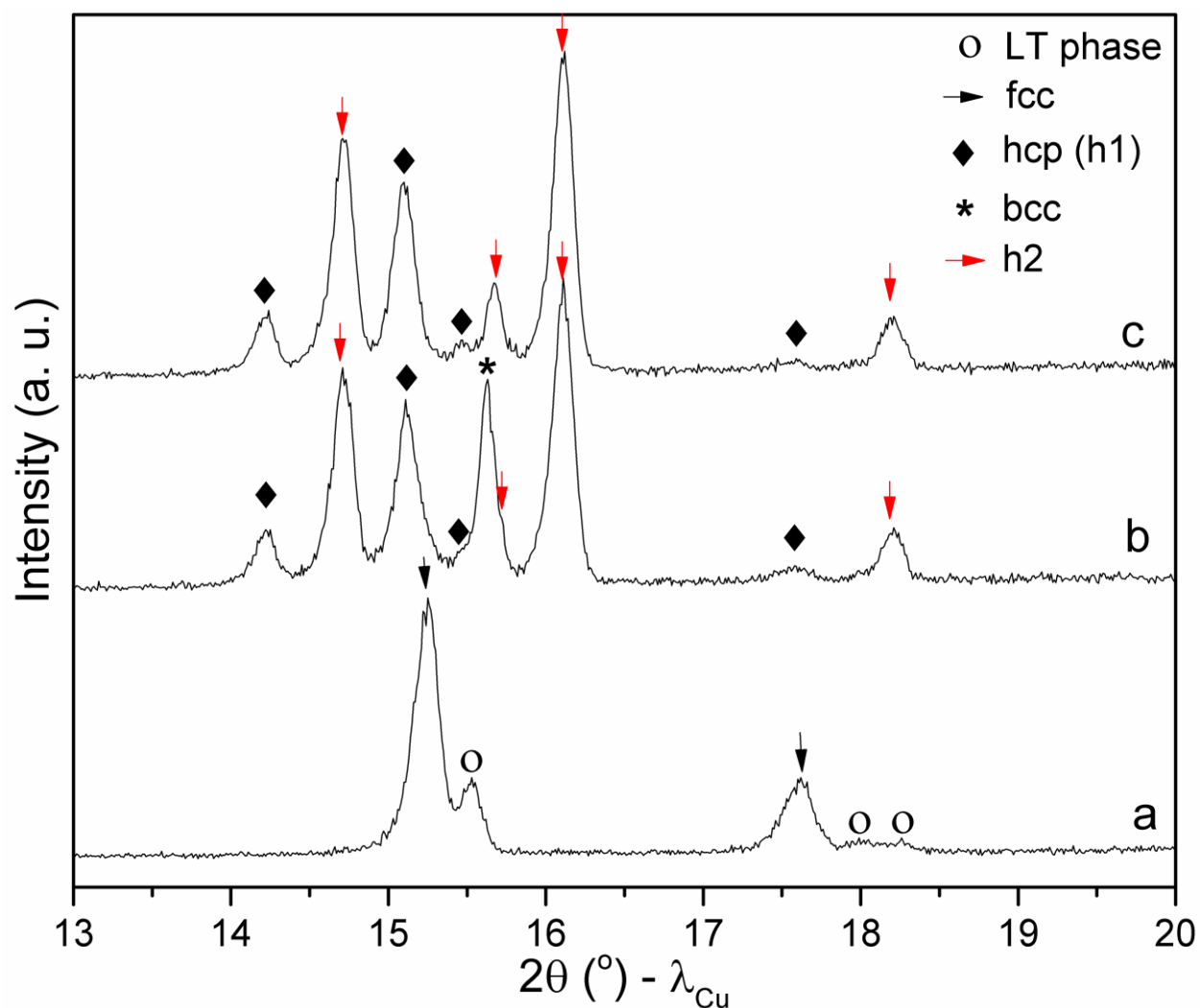


Fig. S2. The high-temperature phase evolution in NaCB₁₁H₁₂: (a) 356 K XRPD pattern (CuK α radiation) with the presence of high-temperature fcc phase and a small amount of low-temperature (LT) orthorhombic phase. (b) 428 K XRPD pattern indicating the formation of body-centered-cubic (bcc) phase and two hexagonal phases, (hexagonal-close-packed (hcp)) h1 and hexagonal h2. (c) 428 K XRD pattern with extended time showing only the two hexagonal phases (h1 and h2). The tentative lattice parameters of these phases at 428 K can be indexed as $a=8.011$ Å for the bcc phase, $a=7.185$ Å and $c=17.19$ Å for the hcp (h1) phase, and $a=6.945$ Å and $c=16.49$ Å for the h2 phase. These phases all revert back to the ordered orthorhombic phase upon cooling.